

# Structural Study of Non-Premixed Tubular Hydrocarbon Flames

Shengteng Hu<sup>1</sup> and Robert W. Pitz<sup>2</sup>

*Mechanical Engineering Department, Vanderbilt University, Nashville, TN 37235 USA*

**Tubular non-premixed flames are formed by a uniquely-designed opposed tubular burner. Structural measurements of hydrocarbon flames are conducted using the laser-induced Raman scattering method. Temperature and major species concentrations are recorded for flames produced by 30% CH<sub>4</sub>/N<sub>2</sub> and 15% C<sub>3</sub>H<sub>8</sub>/N<sub>2</sub> burning against air. Numerical simulations of these flames with detailed chemistry show good agreement between the measured and simulated results. Comparing with the numerical results of the tubular flames to the opposed-jet planar flames, it is shown that curvature towards the fuel stream strengthens the C<sub>3</sub>H<sub>8</sub> flames (fuel Lewis number > 1) and weakens the CH<sub>4</sub> flames (fuel Lewis number ≈ 1).**

## I. Introduction

The effects of stretch on premixed, non-premixed and partially-premixed laminar flames are well understood, a courtesy of the efforts by many years of study from researchers all over the world.<sup>1,2</sup> Tubular flames allow the investigation of curvature effects in addition to the flame stretch.<sup>3</sup> There were many studies on premixed tubular flames, either experimental,<sup>4,8</sup> numerical<sup>9,10</sup> or theoretical.<sup>11,12</sup> However, reports<sup>13</sup> on non-premixed tubular flames are extremely rare, primarily because of the difficulties in establishing such a flame. By installing a nozzle along the symmetrical axis of the tubular burner as a second, radially-outwardly flowing reactant source, non-premixed and partially-premixed tubular flames subject to well-controlled aerodynamic straining and flame curvature can be created.

Studies of curvature effects on non-premixed laminar flames have been carried out on the vortex flames formed by perturbing the flat opposed-jet flame with a syringe tube<sup>14-18</sup> or a bluff body<sup>19</sup> and on the flame tip of the Burke-Schumann flame<sup>20-22</sup>. These flames all suffered from a non-constant curvature and were unsteady in some cases, which make the effects of curvature difficult to identify. An opposed tubular burner can circumvent these difficulties. The important features of the opposed tubular burner can be summarized as: 1) Curvature and flame stretch can be varied independently because their directions are orthogonal to each other. 2) Curvature throughout the flame front is uniform because the diameter of the flame tube is constant at a given condition. 3) The flow field is simple and all quantities can be described as functions of radial location only, which is preferred by both experimentalists and modelers. 4) Both concave and convex curvature can be easily established under well-controlled conditions. Due to these advantages, the opposed tubular burner deserves more attention as a useful tool for fundamental research on combustion science. This study is focused on the structural measurements of the opposed tubular non-premixed flames generated by hydrocarbon fuels.

Structural studies on hydrogen opposed tubular flames, where the fuel stream Lewis is less than one, have been reported.<sup>23,24</sup> Profiles of temperature and major species concentrations were measured using Raman spectroscopy. It was shown that the effects of curvature coupled with the Lewis number effects (Lewis number is defined as the ratio between the mixture thermal diffusivity and the mass diffusivity of the deficient reactant species) are affecting flame properties, which was consistent with the previous numerical study.<sup>25</sup> It is natural to extend the work to opposed tubular non-premixed flames produced by hydrocarbon fuels (CH<sub>4</sub> or C<sub>3</sub>H<sub>8</sub>). Together with the previous studies, both the unity and non-unity Lewis number cases are completely covered. Numerical simulation with detailed chemistry is also carried out in this study. The experimental data serve as an evaluation of the reaction mechanisms. In addition, this study helps on developing an in-depth understanding of the effects of curvature on laminar non-premixed flames.

---

<sup>1</sup> Graduate Student, Mechanical Engineering Department, Student Member.

<sup>2</sup> Chair and Professor, Mechanical Engineering Department, Associate Fellow.

## II. Experimental Setup

Visible Raman spectroscopy is used to measure the temperature and concentrations of major species. The previous experimental system<sup>23</sup> is used for this work with some minor upgrades. A detailed schematic is shown in Fig. 1. The laser beam (Continuum Powerlite 9010, frequency-doubled, pulsed Nd:YAG laser, ~355 mJ/pulse @ 10 Hz) passes through a rotatable zero order waveplate followed by a thin film plate polarizer mounted at its Brewster angle to enable continuous adjustment of the beam energy. The attenuated beam then goes through a pulse stretcher similar to that depicted by Kojima and Nguyen<sup>26</sup>. The laser beam is split into 3 sets of beams that are trapped in 3 optical ring cavities. Each beam experiences a different time delay. A laser pulse of approximately 150 ns long is subsequently produced. This allows a pulsed laser with much higher power to be used where laser-induced breakdown is avoided.

A small fraction of the laser beam is reflected by a plane window mounted at a small angle to monitor the laser pulse to pulse energy variation. A pyroelectric joulemeter (Coherent Moletron J50) with a ND filter and a quartz diffuser mounted in the front is utilized to detect this light.

The pulse energy is used later on in the data reduction process. The main laser beam is focused by a 300 mm focal-length lens down to 150  $\mu\text{m}$  in diameter at the focal point. The scattered Raman light is collected at 90° using a f/2 achromat (75 mm diameter) focused by a second achromat (f/7.5) onto the entrance slit of the spectrometer<sup>27</sup>. The light is then dispersed by a 600 groove/mm grating and focused to a liquid-nitrogen cooled, back-illuminated CCD camera (1024  $\times$  1024 pixels) by a 0.65 m focusing mirror. The magnification ratio of the whole system is 3.08, which is determined by a 6 lines/mm Ronchi grating. The spatially resolved line imaging Raman signal is recorded by the camera. The sample volume (4.06 mm) is divided to 26 sections, which gives a spatial resolution of 156  $\mu\text{m}$ . The ability of the system to resolve this spatial resolution is confirmed by back illuminating the 6 lines/mm Ronchi grating placed in the sample zone. The laser beam passes 4.7 mm away from the burner's axis of symmetry. The location of each data point in the radial direction is calculated based on the separation distance and its position along the laser beam from the point of symmetry.

The CCD camera is gated by a heated ferroelectric liquid crystal shutter (40  $\mu\text{s}$ ) and a mechanical shutter (4.0 ms) to reduce the background flame emission. The Rayleigh scattered light is blocked by an OG-550 filter (3 mm thickness). The flame illumination in the infrared region is blocked by an infrared filter (750 nm cutoff, 3 mm thickness). 600 single-pulse Raman signals are integrated on the CCD chip to produce one Raman image. The tubular burner is translated several times along the laser beam direction to cover the entire flame. A set of representative Raman spectra at different radial locations is shown in Figure 2, where  $R_s$  refers to the radius of curvature of the stagnation surface under the cold flow conditions<sup>12,23</sup> and  $k$  is the flame stretch defined elsewhere.<sup>12</sup> Hydrocarbon fuels are known to produce interferences mainly from  $\text{C}_2$  LIF.<sup>28</sup> As shown in Fig. 2-(b), (f) and (g),  $\text{C}_2$  LIF interferes with  $\text{N}_2$  signal, and this makes the data interpolation in the fuel rich regions difficult. All the flames studied here are blue indicating that no visible soot is present. In addition to the  $\text{C}_2$  LIF, strong interference that comes from the scattering of the reflected laser light by the window of the burner exit port off the wall of the inner nozzle is observed at some locations, which is shown as a broadband feature in the spectra, e.g. Fig. 2-(b). As a result, most of the data in the small radius regions are discarded with only two exceptions, which are shown later. The laser beam passes the flame front twice, so the two sets of identical Raman data are available for each experimental condition. In the results shown hereafter, the two data sets are shown in the same plot. This demonstrates the reliable performance of both the tubular burner and the measurement system.

Calibration flames of hydrogen-air, hydrogen-air- $\text{CO}_2$  and hydrogen-air-CO are produced using a Hencken burner (12.5 mm diameter multi-element matrix surrounded by a 4.3 mm wide  $\text{N}_2$  co-flow annulus). Equilibrium

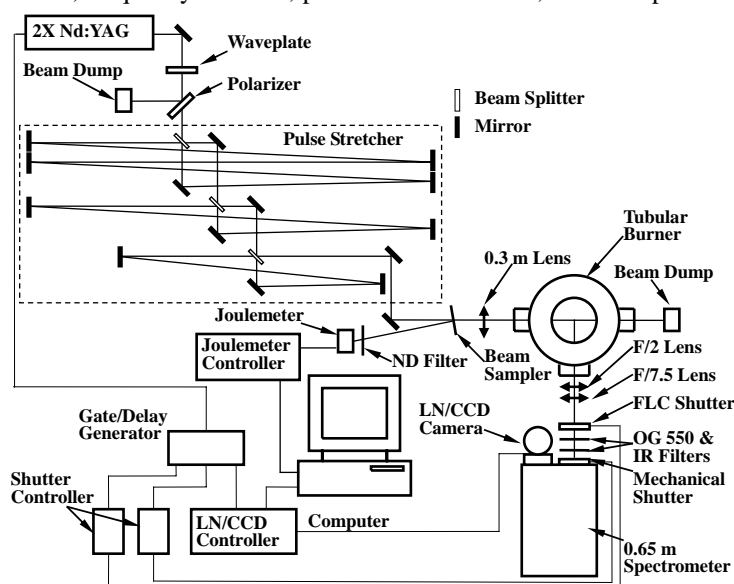


Figure 1. Schematic of the visible Raman scattering system

conditions are assumed in the flame where the laser beam passes 18 mm downstream and the adiabatic flame temperature is used to correlate the calibration factors for each individual species. The uncertainties of the mass flow meters used in the calibration are  $\pm 1\%$  of full scale. The accuracy of the temperature measurement is estimated to be less than  $\pm 5\%$  by comparing the Raman derived temperature with the calculated adiabatic flame temperature of the calibration flames.

### III. Results and discussions

An opposed tubular burner with outer nozzle diameter of 30 mm and inner nozzle diameter of 6.4 mm is employed, where the heights of both nozzles are 20 mm (Fig. 3). A detailed description of the opposed tubular burner can be found elsewhere.<sup>8,23</sup> Two sets of experiments with different fuel type ( $\text{CH}_4$  and  $\text{C}_3\text{H}_8$ ) are conducted. Three parameters are used to describe each experimental case, which are 1) the stretch rate,  $k$ , whose definition can be found in the previous reports;<sup>12,23</sup> 2) the fuel dilution ratio; 3) the radius of the stagnation surface, the equation of which can also be found in the previous reports.<sup>12</sup> In the first set of experiments, flames that use 30%  $\text{CH}_4$  diluted by 70%  $\text{N}_2$  burning against air at various stretch rates are investigated. In the second set of experiments, flames that use 15%  $\text{C}_3\text{H}_8$  diluted by 85%  $\text{N}_2$  burning against air at various stretch rates are studied. For both cases, the exit velocities of the inner and outer nozzle are matched such that the calculated cold flow stagnation surface is located at  $R_s = 6.5$  mm to produce a constant flame curvature. Concentrations of major species ( $\text{CO}_2$ ,  $\text{H}_2\text{O}$ ,  $\text{N}_2$ ,  $\text{O}_2$ ,  $\text{CH}_4$  and  $\text{C}_3\text{H}_8$ ) are derived from the Raman spectra. The temperature distribution is obtained by invoking the ideal gas law

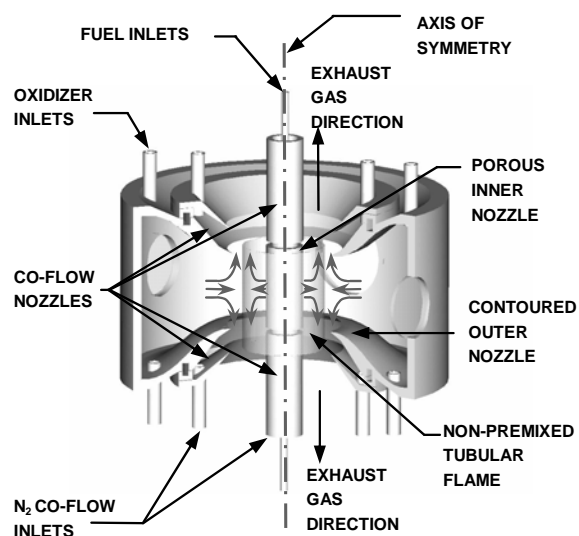


Figure 3. Schematic of the opposed tubular burner

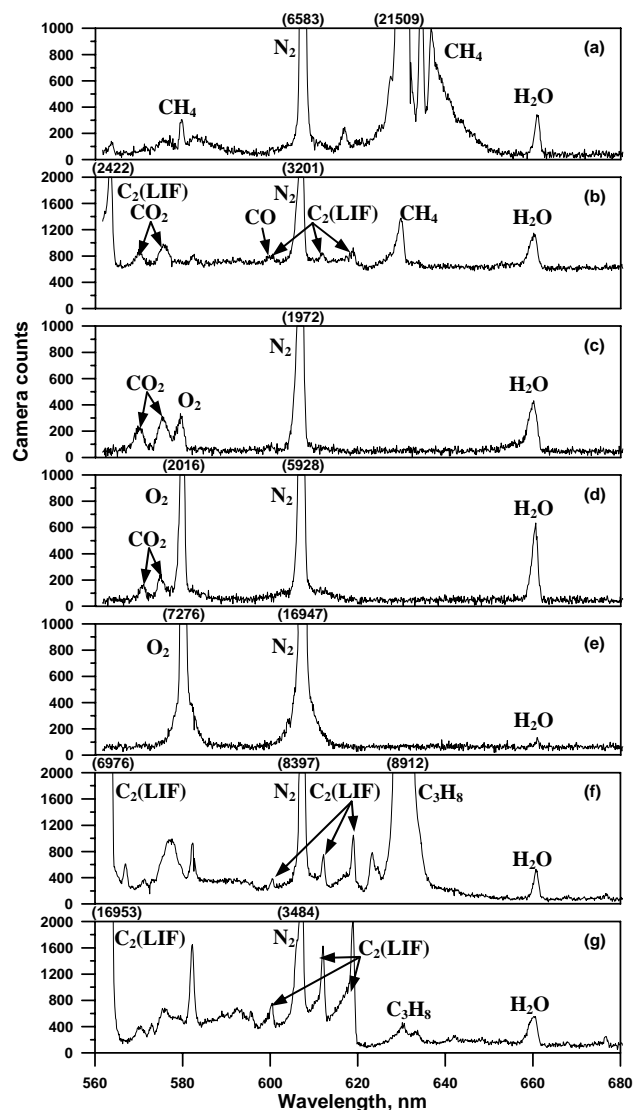


Figure 2. Raman spectra of the opposed tubular flame at different radial locations. (a) - (e)  $k=122 \text{ s}^{-1}$ ,  $R_s = 6.5$  mm, 30%  $\text{CH}_4/\text{N}_2$ -air flame; (f) and (g)  $k=100 \text{ s}^{-1}$ ,  $R_s = 6.5$  mm, 15%  $\text{C}_3\text{H}_8/\text{N}_2$ -air flame. (a)  $r = 5.2$  mm,  $T = 563$  K; (b)  $r = 7.0$  mm,  $T = 1717$  K; (c)  $r = 7.6$  mm,  $T = 1731$  K; (d)  $r = 8.6$  mm,  $T = 844$  K; (e)  $r = 10.5$  mm,  $T = 300$  K; (f)  $r = 5.2$  mm; (g)  $r = 6.7$  mm. (note the different y scale in (b), (f) and (g))

assuming constant pressure. The flames studied in this work are all concave towards the fuel stream, i.e. the fuel is issued from the burner's inner nozzle. Numerical simulations of the opposed tubular non-premixed flames are conducted using a modified Oppdif code,<sup>8</sup> where plug flow boundary conditions are assumed. Various reaction mechanisms are used which are detailed in the discussion below. All the calculation results shown hereafter have no heat transfer at the burner boundary. The experimental data are shifted about 1.6 mm in the radial direction towards smaller values to match with the calculations.

This difference in radial location is due to the difference in the boundary conditions between the experiments and simulations.

### A. Methane Flames

Figure 4-8 show the Raman-derived profiles of temperature and major species concentrations for the non-premixed opposed tubular flames (30%  $\text{CH}_4/\text{N}_2$  vs. air) with stretch rates ranging from  $k = 41$  to  $122 \text{ s}^{-1}$ . The numerical simulated profiles are shown as solid lines in the figures. GRI 3.0<sup>29</sup> mechanisms are used in the numerical simulations except in Fig. 5 where simulated temperature profiles using the Kee,<sup>30</sup> C1,<sup>31</sup> C2<sup>31</sup> and GRI 3.0 mechanisms are shown. The Kee and C1 mechanisms model hydrocarbons with one carbon atom only; the C2 and GRI 3.0 mechanisms include up to two carbon atoms. Multicomponent formulation for transport properties is adopted. It is seen that the computed profiles agree well with the experimental measurements and the results are

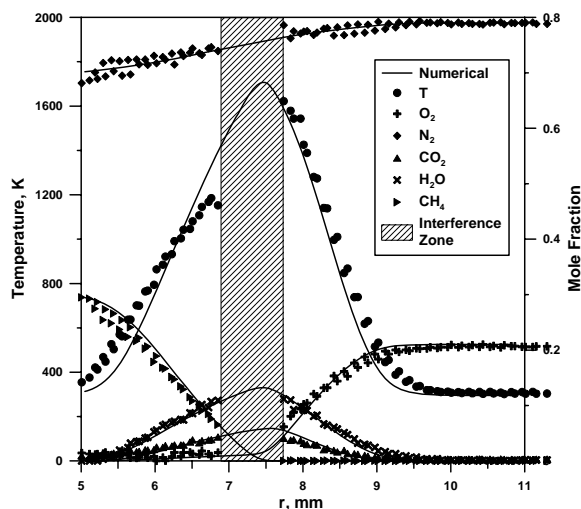


Figure 4. Measured and calculated temperature and major species mole fraction profiles as functions of radius for a 30%  $\text{CH}_4/\text{N}_2$ -air non-premixed tubular flame at  $k=122 \text{ s}^{-1}$ ,  $R_s=6.5 \text{ mm}$ .

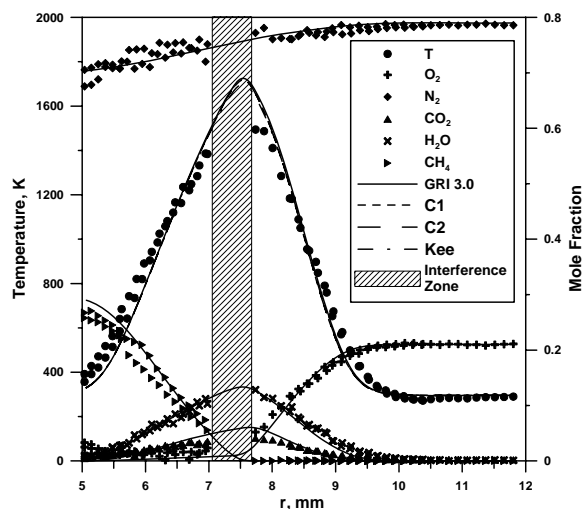


Figure 5. Measured and calculated temperature and major species mole fraction profiles as functions of radius for a 30%  $\text{CH}_4/\text{N}_2$ -air non-premixed tubular flame at  $k=102 \text{ s}^{-1}$ ,  $R_s=6.5 \text{ mm}$ .

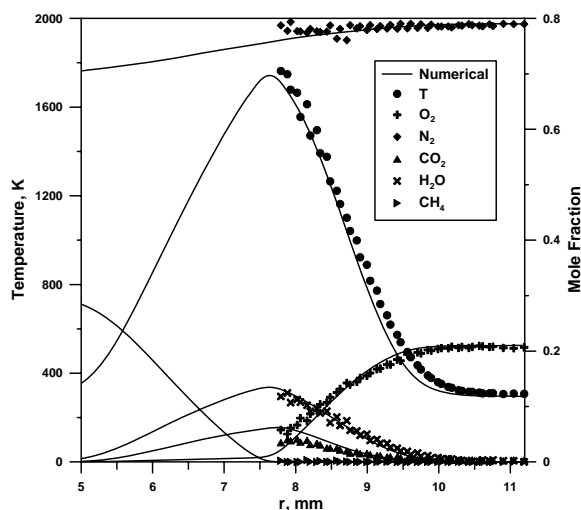


Figure 6. Measured and calculated temperature and major species mole fraction profiles as functions of radius for a 30%  $\text{CH}_4/\text{N}_2$ -air non-premixed tubular flame at  $k=81 \text{ s}^{-1}$ ,  $R_s=6.5 \text{ mm}$ .

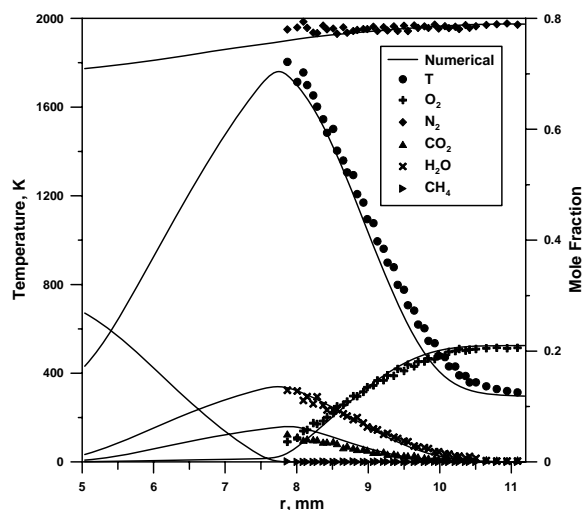


Figure 7. Measured and calculated temperature and major species mole fraction profiles as functions of radius for a 30%  $\text{CH}_4/\text{N}_2$ -air non-premixed tubular flame at  $k=61 \text{ s}^{-1}$ ,  $R_s=6.5 \text{ mm}$ .

found to be independent of the specific chemical mechanisms as might be expected for non-premixed flames. The difference among the predicted temperature profiles is minimal.

As shown in Fig. 4 and 5, the flame thicknesses at relatively-high stretch rates ( $k > 100 \text{ s}^{-1}$ ) are small comparing to other flames shown later. The regions where  $\text{C}_2$  LIF interferes with the Raman signal are also small. As a result, temperature and species concentration data can be made available with reduced degree of accuracy for locations where the radii are small as shown in Fig. 4 and 5 (see the increased scattering in the measurements for  $r < 7 \text{ mm}$ ). The regions where interferences become severe are marked as shadows and data are not shown due to the great uncertainty encountered in the attempt to reduce the data. As the stretch rate decreases, the flame becomes thicker as shown in Fig. 6-8. Severe interferences are observed at small radial locations, and therefore the data are discarded.

### B. Propane Flames

The Raman-derived profiles of temperature and major species concentrations for the non-premixed opposed

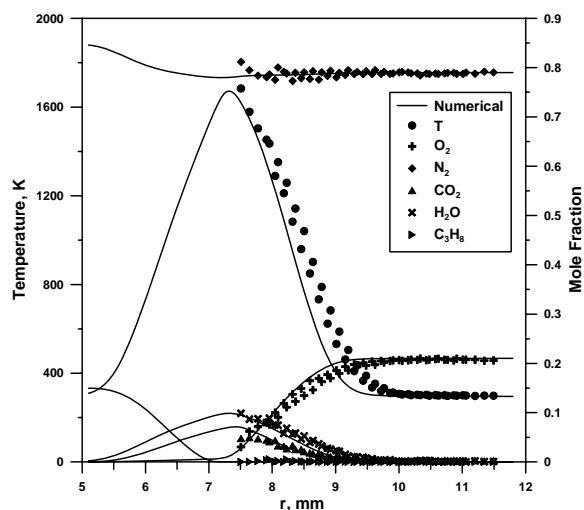


**Figure 9.** Measured and calculated temperature and major species mole fraction profiles as functions of radius for a 15%  $\text{C}_3\text{H}_8/\text{N}_2$ -air non-premixed tubular flame at  $k=100 \text{ s}^{-1}$ ,  $R_s=6.5 \text{ mm}$ .

tubular flames (15%  $\text{C}_3\text{H}_8/\text{N}_2$  vs. air) with stretch rates ranging from  $k = 33$  to  $100 \text{ s}^{-1}$  are shown in Fig. 9-13. The numerical simulated profiles are shown as solid lines in the figures. The San Diego mechanism<sup>32</sup>, which models up to three carbon atoms, is used in the simulations. Mixing-average formulation is utilized for the  $\text{C}_3\text{H}_8$  flames to reduce the computational cost. The experimental spectra of the propane flames suffer from  $\text{C}_2$  LIF interferences more severely than the ones of the methane flames due to the higher concentrations of  $\text{C}_2$  species in the fuel rich streams. A set of representative spectra are shown in Fig. 2-(f) and (g). As a result, only data on the oxidizer stream side of the flame surface are made available, and the data at smaller radial locations on the fuel stream side are discarded. The computed profiles agree well with the experimental measurements. The difference between the measured and predicted temperature profiles is minimal.

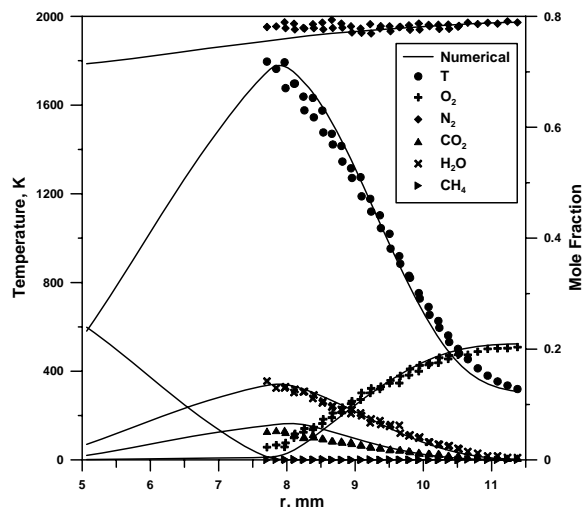


**Figure 8.** Measured and calculated temperature and major species mole fraction profiles as functions of radius for a 30%  $\text{CH}_4/\text{N}_2$ -air non-premixed tubular flame at  $k=41 \text{ s}^{-1}$ ,  $R_s=6.5 \text{ mm}$ .

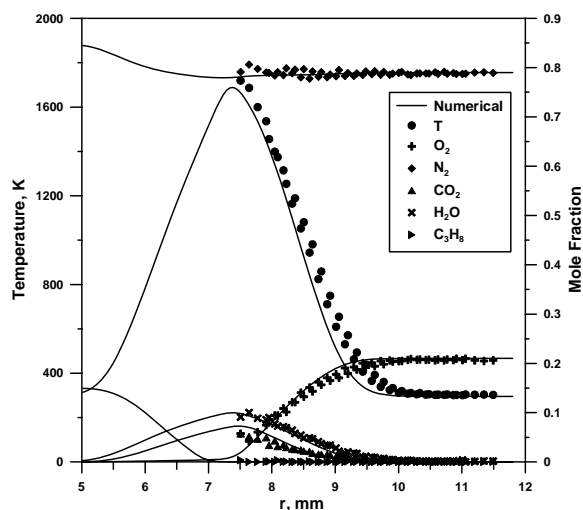


**Figure 10.** Measured and calculated temperature and major species mole fraction profiles as functions of radius for a 15%  $\text{C}_3\text{H}_8/\text{N}_2$ -air non-premixed tubular flame at  $k=84 \text{ s}^{-1}$ ,  $R_s=6.5 \text{ mm}$ .

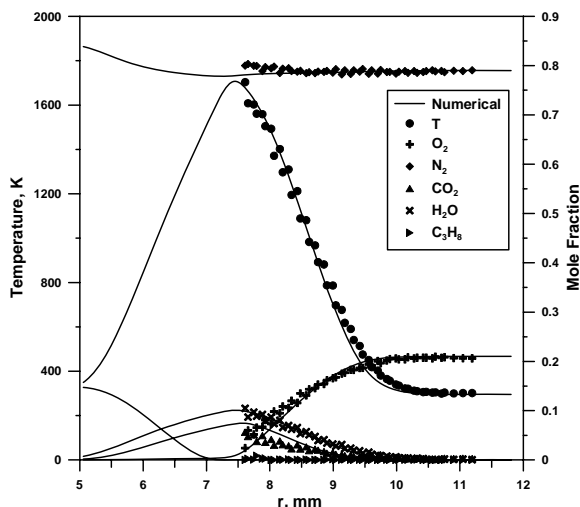


Figure 11. Measured and calculated temperature and major species mole fraction profiles as functions of radius for a 15%  $C_3H_8/N_2$ -air non-premixed tubular flame at  $k=67 \text{ s}^{-1}$ ,  $R_s=6.5 \text{ mm}$ .

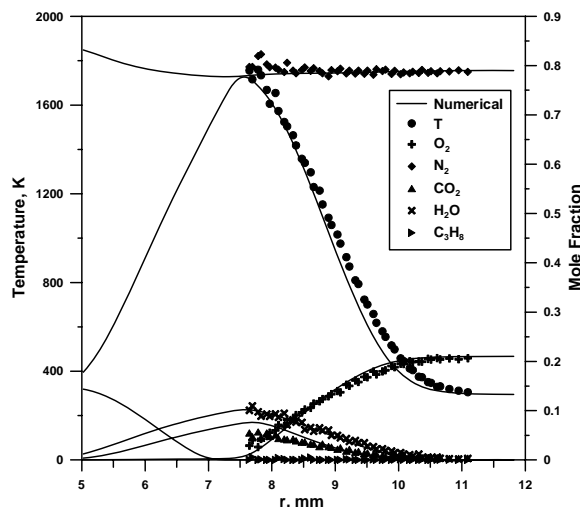


Figure 12. Measured and calculated temperature and major species mole fraction profiles as functions of radius for a 15%  $C_3H_8/N_2$ -air non-premixed tubular flame at  $k=50 \text{ s}^{-1}$ ,  $R_s=6.5 \text{ mm}$ .

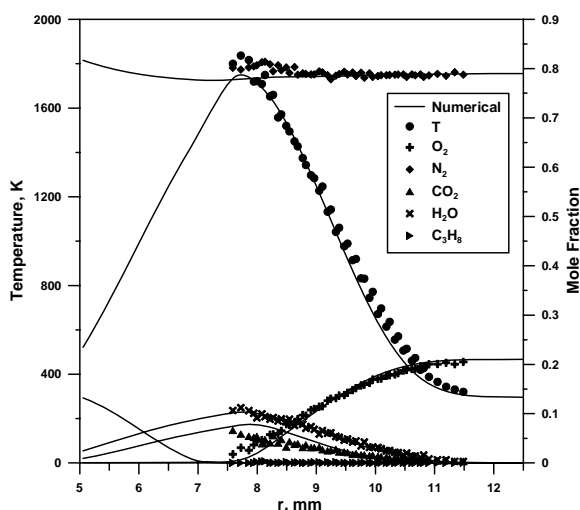


Figure 13. Measured and calculated temperature and major species mole fraction profiles as functions of radius for a 15%  $C_3H_8/N_2$ -air non-premixed tubular flame at  $k=33 \text{ s}^{-1}$ ,  $R_s=6.5 \text{ mm}$ .

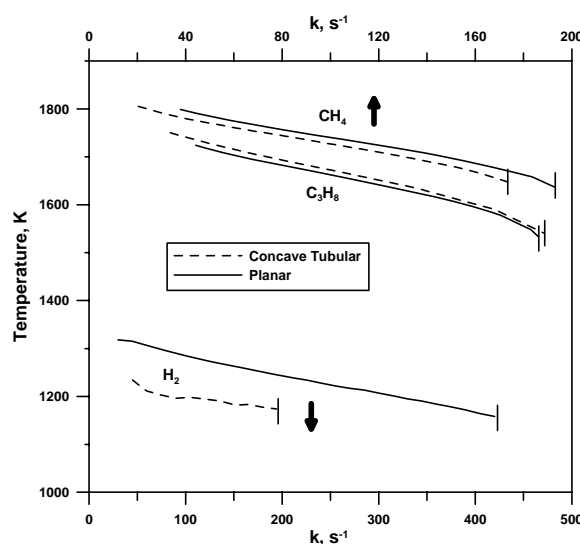


Figure 14. Calculated maximum flame temperature as functions of stretch rate of the opposed jet planar and tubular flames using 15%  $H_2/N_2$ , 30%  $CH_4/N_2$  and 15%  $C_3H_8/N_2$  showing the different effects of curvature (note  $H_2$  uses the lower x-axis and  $CH_4/C_3H_8$  use the upper x-axis).

Figure 14 shows the variations of the calculated maximum flame temperature of the tubular and opposed-jet planar flames as functions of stretch rate. The maximum flame temperatures decrease with increasing stretch rate as a result of increased degree of combustion incompleteness. However, curvature shows opposite effects on the maximum temperatures of the methane and propane flames. For  $CH_4$  flame, the opposed jet planar flame demonstrates higher flame temperature than the opposed tubular flame, while for  $C_3H_8$  flame, the opposite stands. The effects of Lewis number coupled with curvature are believed to be responsible for such a difference as suggested by earlier studies.<sup>14-19,23-25</sup>. The Lewis number of the oxidizer stream is close to unity and not varied in these experiments. The non-unity Lewis number of the fuel mixture controls the diffusion of the fuel to the flame surface. When Lewis number of the fuel stream is greater than one ( $C_3H_8/N_2$ ), curvature concave toward the fuel stream promotes combustion and flames exhibit higher peak temperature, which is consistent with the previous studies.<sup>23-25</sup> The Lewis number of  $CH_4/N_2$  mixture is

close to one, but the  $\text{CH}_4$  flames act like flames with Lewis number less than one ( $\text{H}_2$  flames<sup>23</sup>), i.e. curvature concave toward the fuel stream retards combustion and flames exhibit lower peak temperature. It is surprising to see from the numerical results of Fig. 13 that the temperature difference between the propane flame curves is so small considering the Lewis number of the  $\text{C}_3\text{H}_8/\text{N}_2$  mixture is much larger than one.

#### IV. Conclusion

Non-premixed tubular hydrocarbon flames are established using a uniquely-designed opposed tubular burner. Laser-induced Raman spectroscopy is applied to both methane and propane flames. Temperature and major species concentrations ( $\text{CO}_2$ ,  $\text{H}_2\text{O}$ ,  $\text{N}_2$ ,  $\text{O}_2$ ,  $\text{CH}_4$  and  $\text{C}_3\text{H}_8$ ) are reported with good resolution. Due to the interferences from the  $\text{C}_2$  LIF and the scattering of the inner wall, only data on the oxidizer side are made available in most cases. Numerical simulations of the measured flames using various reaction mechanisms are conducted. Shown in the methane flame simulation, the specific reaction mechanism has little effect on the simulation results of temperature and major species concentrations. The experimental data and numerical predictions agree well. Comparison of the peak flame temperatures from numerical calculations of the opposed jet planar and opposed tubular flames of different fuels confirms the conclusion in the previous study, i.e. concave curvature strengthens flame when fuel mixture  $Le > 1$ .

#### Acknowledgments

The authors would like to acknowledge the financial support from NASA (NASA Grant No: NNC04AA14A) with John Brooker as the technical monitor. The assistance from Yu Wang is highly appreciated.

#### References

- <sup>1</sup>Seshadri, K., Puri, I. and Peters, N., "Experimental and Theoretical Investigation of Partially Premixed Diffusion Flames at Extinction," *Combustion and Flame*, Vol. 61, 1985, 237-249.
- <sup>2</sup>Law, C. K., "Dynamics of Stretched Flames," *Proceedings of the Combustion Institute*, Vol. 22, 1988, 1381-1402.
- <sup>3</sup>Ishizuka, S., "Characteristics of Tubular Flames," *Progress in Energy and Combustion Science*, Vol. 19, No. 3, 1993, 187-226.
- <sup>4</sup>Ishizuka, S., "An Experimental Study on Extinction and Stability of Tubular Flames," *Combustion and Flame*, Vol. 75, 1989, 367-379.
- <sup>5</sup>Kitano, M., Kobayashi, H. and Otsuka, Y., "A Study of Cylindrical Premixed Flames with Heat Loss," *Combustion and Flame*, Vol. 76, No. 1, 1989, 89-105.
- <sup>6</sup>Kobayashi, H. and Kitano, M., "Extinction Characteristics of a Stretched Cylindrical Premixed Flame," *Combustion and Flame*, Vol. 76, 1989, 285-295.
- <sup>7</sup>Ogawa, Y., Saito, N. and Liao, C., "Burner Diameter and Flammability Limit Measured by Tubular Flame Burner," *Proceedings of the Combustion Institute*, Vol. 27, 1998, 3221-3227.
- <sup>8</sup>Mosbacher, D. M., Wehrmeyer, J. A., Pitz, R. W., Sung, C.-J. and Byrd, J. L., "Experimental and Numerical Investigation of Premixed Tubular Flames," *Proceedings of the Combustion Institute*, Vol. 29, 2002, 1479-1486.
- <sup>9</sup>Dixon-Lewis, G., Giovangigli, V., Kee, R. J., Miller, J. A., Rogg, B., Smooke, M. D., Stahl, G. and Warnatz, J., "Numerical Modeling of the Structure and Properties of Tubular Strained Laminar Premixed Flames," *Progress in Astronautics and Aeronautics*, Vol. 131, 1991, 125-144.
- <sup>10</sup>Nishioka, M., Inagaki, K., Ishizuka, S. and Takeno, T., "Effects of Pressure on Structure and Extinction of Tubular Flame," *Combustion and Flame*, Vol. 86, No. 1-2, 1991, 90-100.
- <sup>11</sup>Libby, P., Peters, N. and Williams, F. A., "Cylindrical Premixed Laminar Flames," *Combustion and Flame*, Vol. 75, 1989, 265-280.
- <sup>12</sup>Wang, P., Wehrmeyer, J. A. and Pitz, R. W., "Stretch Rate of Tubular Premixed Flames," *Combustion and Flame*, Vol. 145, 2006, 401-414.
- <sup>13</sup>Qian, J. and Law, C. K., "On the Spreading of Unsteady Cylindrical Diffusion Flames," *Combustion and Flame*, Vol. 110, No. 1-2, 1997, 152-162.
- <sup>14</sup>Katta, V. R., Carter, C. D., Fiechtner, G. J., Roquemore, W. M., Gord, J. R. and Rolon, J. C., "Interaction of a Vortex with a Flat Flame Formed between Opposing Jets of Hydrogen and Air," *Proceedings of the Combustion Institute*, Vol. 27, 1998, 587-594.
- <sup>15</sup>Lee, J. C., Frouzakis, C. E. and Boulouchos, K., "Numerical Study of Opposed-Jet  $\text{H}_2$ /Air Diffusion Flame - Vortex Interactions," *Combustion Science and Technology*, Vol. 158, 2000, 365-388.
- <sup>16</sup>Yoshida, K. and Takagi, T., "Structural Studies of Locally Strained Diffusion Flames," *JSME International Journal, Series B*, Vol. 46, No. 1, 2003, 190-197.
- <sup>17</sup>Yoshida, K. and Takagi, T., "Transient Local Extinction and Reignition Behavior of Diffusion Flames Affected by Flame Curvature and Preferential Diffusion," *Proceedings of the Combustion Institute*, Vol. 27, 1998, 685-692.

- <sup>18</sup>Takagi, T., Yoshikawa, Y., Yoshida, K., Komiyama, M. and Kinoshita, S., "Studies on Strained Non-Premixed Flames Affected by Flame Curvature and Preferential Diffusion," *Proceedings of the Combustion Institute*, Vol. 26, 1996, 1103-1110.
- <sup>19</sup>Finke, H. and Grünefeld, G., "An Experimental Investigation of Extinction of Curved Laminar Hydrogen Diffusion Flames," *Proceedings of the Combustion Institute*, Vol. 28, 2000, 2133-2140.
- <sup>20</sup>Ishizuka, S., "An Experimental Study on the Opening of Laminar Diffusion Flame Tips," *Proceedings of the Combustion Institute*, Vol. 19, 1982, 319-326.
- <sup>21</sup>Im, H. G., Law, C. K. and Axelbaum, R. L., "Opening of the Burke-Schumann Flame Tip and the Effects of Curvature on Diffusion Flame Extinction," *Proceedings of the Combustion Institute*, Vol. 23, 1990, 551-558.
- <sup>22</sup>Greenberg, J. B. and Grodek, F., "Curvature Effects in Burke-Schumann Spray Flame Extinction," *AIAA Journal*, Vol. 41, No. 8, 2003, 1507-1513.
- <sup>23</sup>Hu, S., Wang, P., Pitz, R. W. and Smooke, M. D., "Experimental and Numerical Investigation of Non-Premixed Tubular Flames," *Proceedings of the Combustion Institute*, Vol. 31, in press, 2006.
- <sup>24</sup>Hu, S., Wang, P., Pitz, R. W. and Smooke, M. D., "Curvature Effects in Non-Premixed Tubular Flames," *44th AIAA Aerospace Sciences Meeting and Exhibit*, AIAA-2006-1133, Reno, NV, 2006.
- <sup>25</sup>Wang, P., Hu, S. and Pitz, R. W., "Numerical Investigation of the Curvature Effects on Diffusion Flames," *Proceedings of the Combustion Institute*, Vol. 31, in press, 2006.
- <sup>26</sup>Kojima, J. and Nguyen, Q. V., "Laser Pulse-Stretching with Multiple Optical Ring Cavities," *Applied Optics*, Vol. 41, No. 30, 2002, 6360-6370.
- <sup>27</sup>Osborne, R. J., Wehrmeyer, J. A. and Pitz, R. W., "A Comparison of UV Raman and Visible Raman Techniques for Measuring Non-Sooting Partially Premixed Hydrocarbon Flames," *38th AIAA Aerospace Sciences Meeting and Exhibit*, AIAA-2000-0776, Reno, NV, 2000.
- <sup>28</sup>Barlow, R. S., Carter, C. D. and Pitz, R. W., *Multiscalar Diagnostics in Turbulent Flames*, in Applied Combustion Diagnostics, edited by K. Kohse-Höinghaus and J. B. Jeffries, Taylor & Francis, New York, 2002, 384-407.
- <sup>29</sup>Smith, G. P., Golden, D. M., Frenklach, M., Moriarty, N. W., Eiteneer, B., Goldenberg, M., Bowman, C. T., Hanson, R. K., Song, S., Jr., W. C. G., Lissianski, V. V. and Qin, Z., "Gas Research Institute, Chicago, Illinois," [http://www.me.berkeley.edu/gri\\_mech/](http://www.me.berkeley.edu/gri_mech/).
- <sup>30</sup>Kee, R. J., Grcar, J. F., Smooke, M. D. and Miller, J. A., "Sandia Report 85-8240," Sandia National Laboratories, 1985.
- <sup>31</sup>Peters, N., *Flame Calculations with Reduced Mechanisms - An Outline*, in Reduced Kinetic Mechanisms for Applications in Combustion Systems - Lecture Notes in Physics, edited by N. Peters and B. Rogg, Vol. M15, Springer-Verlag, Berlin, 1993, Ch.1, 3-12.
- <sup>32</sup><http://maeweb.ucsd.edu/~combustion/cermech/>, 2005/06/15.